Electronic Supplementary Material (ESI) for Journal of Materials Chemistry C.

Temperature sensor based on europium polyoxometalate and mesoporous terbium metal-organic framework

Cédric Viravaux,[a] Olivier Oms,[a] Anne Dolbecq,[a] Emma Nassar,[a] Lucas Busson,[a] Caroline Mellot-Draznieks,[b] Rémi Dessapt,[c] Hélène Serier-Brault[c,]* and Pierre Mialane[a,]*

Experimental section

Infrared spectra were recorded on a Nicolet 30 ATR 6700 FT spectrometer.

EDX measurements were performed on a JEOL JSM 5800LV apparatus.

Thermogravimetry analyses (TGA) were performed on a Mettler Toledo TGA/DSC 1, STARe System apparatus under oxygen flow (50 mL min^{-1}) at a heating rate of 5°C min^{-1} up to 700°C. TGA measurements were performed on samples (Tb-TATB and POM@Tb-TATB) which have been washed with water and ethanol and dried overnight.

Powder X-ray diffraction (PXRD) data were obtained on a Bruker D5000 diffractometer using Cu radiation (1.54059 Å).

Single-crystal X-Ray intensity data collection was carried out with a four-circle kappa-axis Bruker D8 Venture diffractometer equipped with Mo wavelength X-ray microsource and photon 100 CMOS detector.

Photoluminescence measurements. Photoluminescence spectra were recorded on a Jobin-Yvon Fluorolog 3 fluorometer equipped with a photomultiplier (excitation source: 450 W Xe arc lamp) using the front face acquisition mode. The emission spectra were corrected for detection and optical spectral response of the spectrofluorimeter and the excitation spectra were weighed for the spectral distribution of the lamp intensity using a photodiode reference detector. The temperature-dependent photoluminescence measurements were recorded on the same spectrometer controlling the temperature by a cryostat coupled with the Fluorolog cooled by liquid nitrogen (right-angle geometry). Lifetimes measurements were measured with the same equipment but the excitation was performed by a UV Xenon flash tube while the time-dependence of the emission was recorded with the photomultiplier.

Computational section

The cubic Tb-TATB crystal structure from Kim *et al.* (*Angew. Chem. Int. Ed.* 2007, **46**, 8230 –8233) was used as the starting model for our computational approach, considering its primitive cell containing 272 Tb atoms. In view of the high level of complexity of this structure in terms of connectivity of the TATB linkers, we decided to use a simplified model as follows. Tb-TATB is reminiscent of MIL-101's crystal structure (G. Férey, C. Mellot-Draznieks, C. Serre, F. Millange, J. Dutour, S. Surblé and I. Margiolaki, Science 2005, **309**, 2040-2042) whereby planar trigonal Tb_4 moieties form a tetrahedral arrangement, namely supertetrahedra (ST). These Tb_4 units are connected through pairs of TATB ligands on each of the six faces of the STs. In Tb-TATB crystal structure, TATB ligands fall into two sub-families, those connecting Tb^{3+} on the outer surface of STs, and those connecting Tb^{3+} in the inner space of STs. In the present work, only outer TATB ligands were taken into account, considering that adsorbed EuW_{10} POMs may not interact with the second type of TATBs which are inaccessible to the guests. Still, due to the severe disorder of the TATB ligands in the cubic space group, the original CIF file misses the explicit description of the triazine-1,3,5-tribenzoic acid ligands and rather reports fully functionalized hexa-benzoïc ligands. The latter results in an artificial over-coordination of the Tb centers. For our simulations, a number of hexa-benzoïc ligands were converted to triazine-1,3,5-tribenzoic acid ligands, thus allowing the coordination of water molecules to the related Tb sites in place of the depleted functional groups. Although such model is indeed an approximation, it allows us to mimic the effective environment of Tb centers as exposed to the pores in the real solid.

For probing the host-guest potential energy surface, we applied a simulated annealing procedure whereby a Monte Carlo Metropolis algorithm is used (N. Metropolis, A. Rosenbluth, M. Rosenbluth, A. Teller and E. Teller, *J. Chem. Phys.* 1953, **21**, 1087.). Each annealing cycle consisted of 50000 independent Monte Carlo steps per POM, initiating each

energy minimization at 1000 K followed by system-cooling to 300 K. Low energy POM adsorption sites were thus identified by searching the configurational space of the {POM, MOF} system as the temperature is slowly decreased. In this conformational search, the POM was treated as a rigid body and host framework as the fixed-atom host. Only the position and orientation of the POM were sampled during the simulated annealing procedure, allowed to visit all possible void volumes of the Tb-TATB's porous crystal structure. Calculations were performed fixing the loading of POM at 4 per unit-cell.

Non-bonded interaction energies between the EuW_{10} POM and the Tb-TATB host were described using the universal forcefield UFF (A. K. Rappé, C. J. Casewit, K. S. Colwell, W. A. Goddard and W. M. Skiff, *J. Am. Chem. Soc.* 1992, **114**, 10024; A. K. Rappé, K. S. Colwell and C. J. Casewit, *Inorg. Chem.* 1993, **32**, 3438) with a real-space cutoff of 43 Å while handling the long-range electrostatic interactions with explicit charges and the Ewald summation technique with a relative precision of 10^{-6}. The atomic charges for the POM and the MOF were calculated by the charge-equilibration method. (A. K. Rappe and W. A. Goddard III. *J. Phys. Chem.* 1995, **95**, 3358). The POM net charge, fixed at -9, was compensated by a net positive charge of the MOF, here +36.

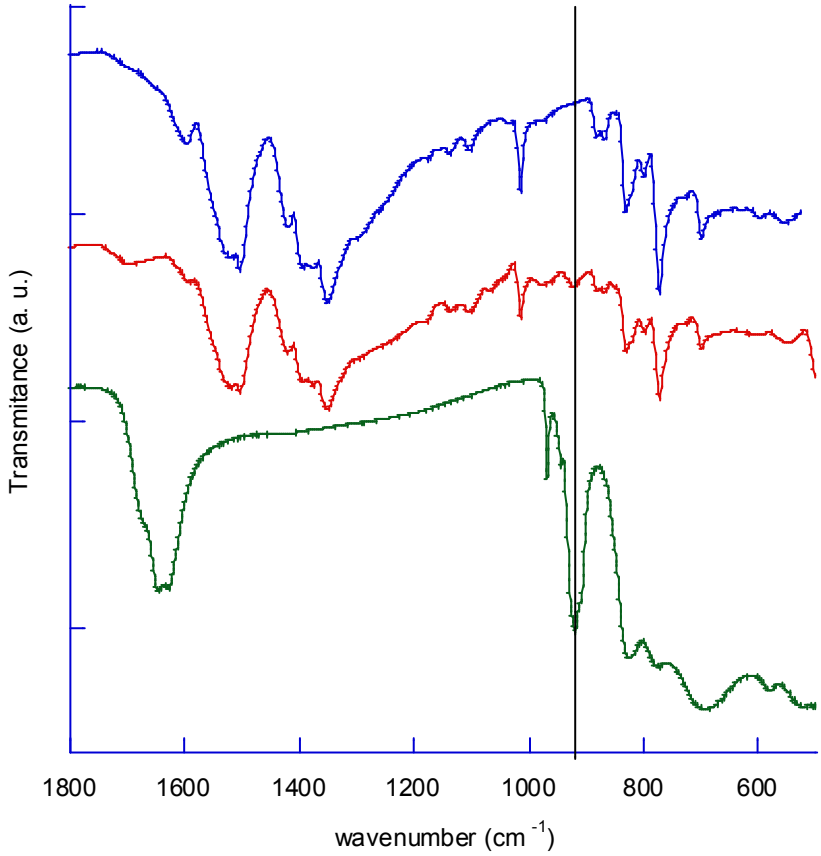

Figure S1: FTIR spectra of Tb-TATB (blue line), EuW_{10} (dark green line) and **19.5wt%EuW_{10}@Tb-TATB** (red line). The vertical black line indicates the W=O vibrations.

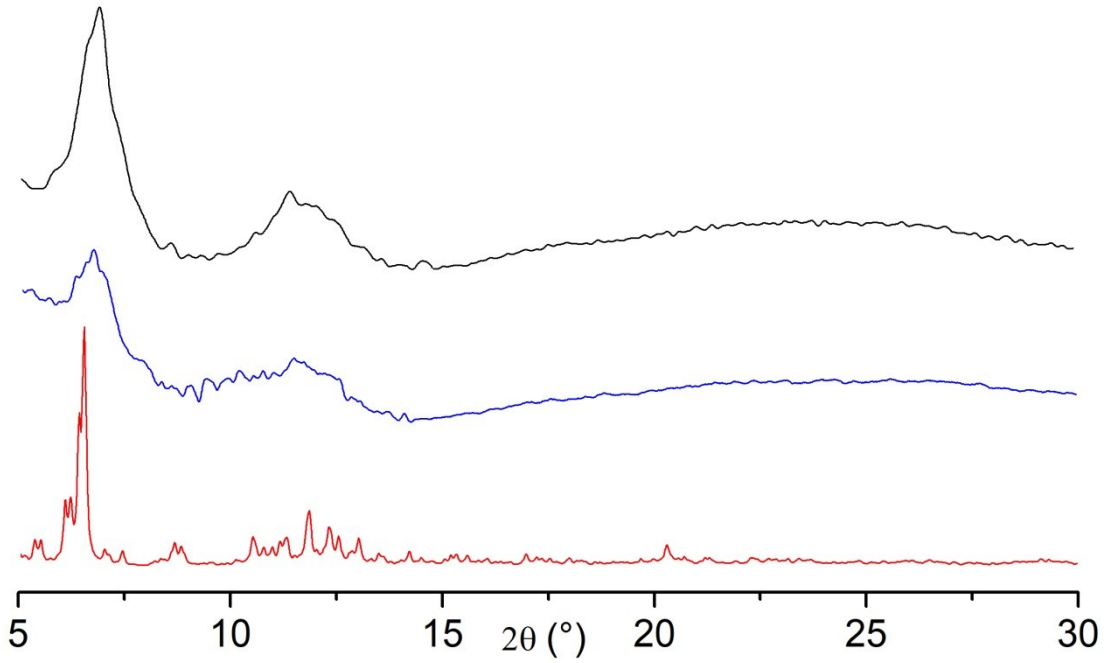

Figure S2: Theoretical (red line) and experimental powder X-Ray diffraction patterns of Tb-TATB (black line) and **19.5wt%EuW$_{10}$@Tb-TATB** (blue line).

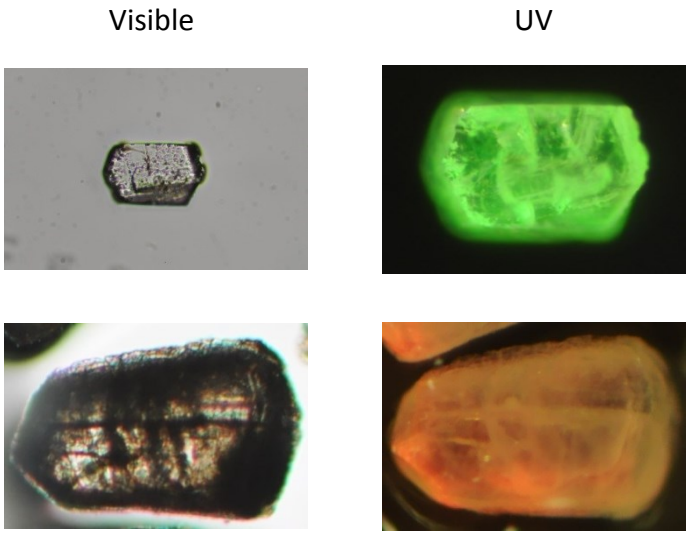

Figure S3: Images of Tb-TATB (top) and **19.5wt%EuW$_{10}$@Tb-TATB** (bottom) under visible or UV-light irradiation (365 nm).

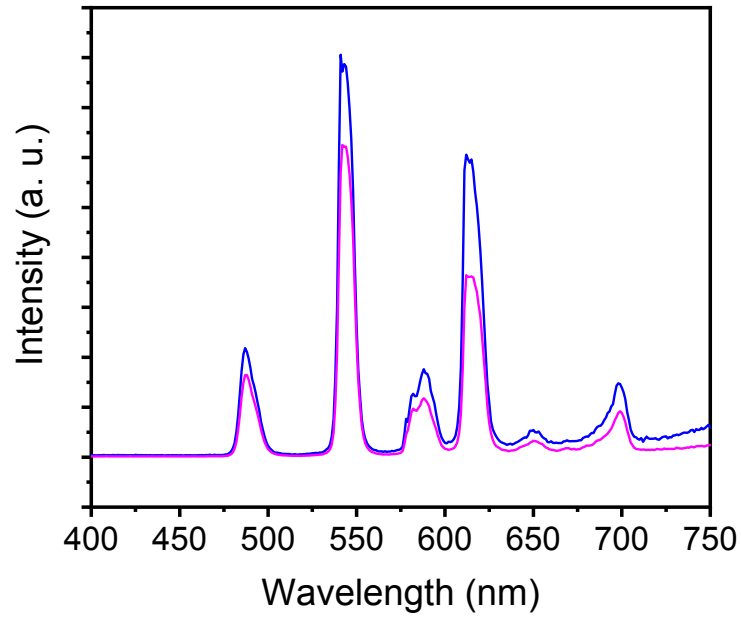

Figure S4: Room-temperature emission spectra of **9.1wt%EuW$_{10}$@Tb-TATB** (pink line) and **19.5wt%EuW$_{10}$@Tb-TATB** (blue line) recorded at λ_{exc} = 330 nm.

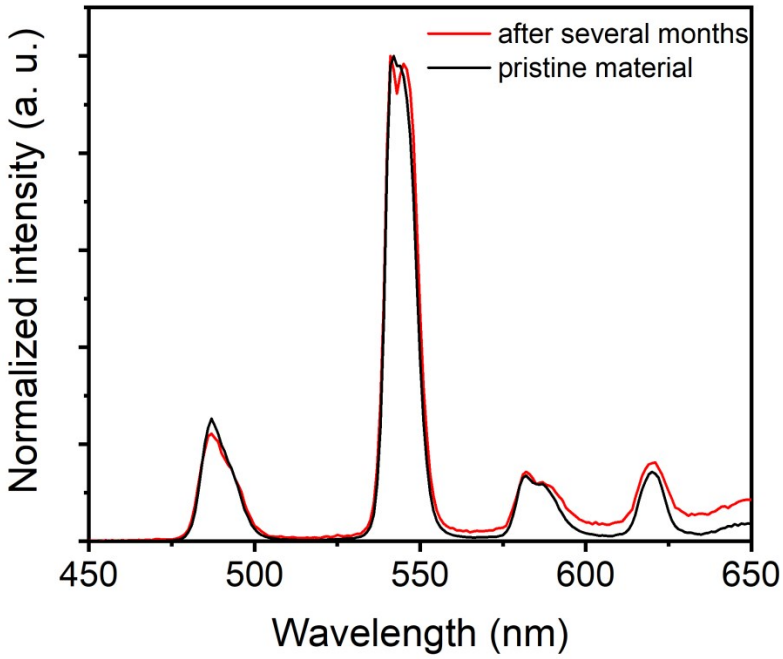

Figure S5: Room-temperature emission spectra at λ_{exc} = 330 nm of pristine **9.1wt%EuW$_{10}$@Tb-TATB** (black line) and **9.1wt%EuW$_{10}$@Tb-TATB** recorded three months later (red line).

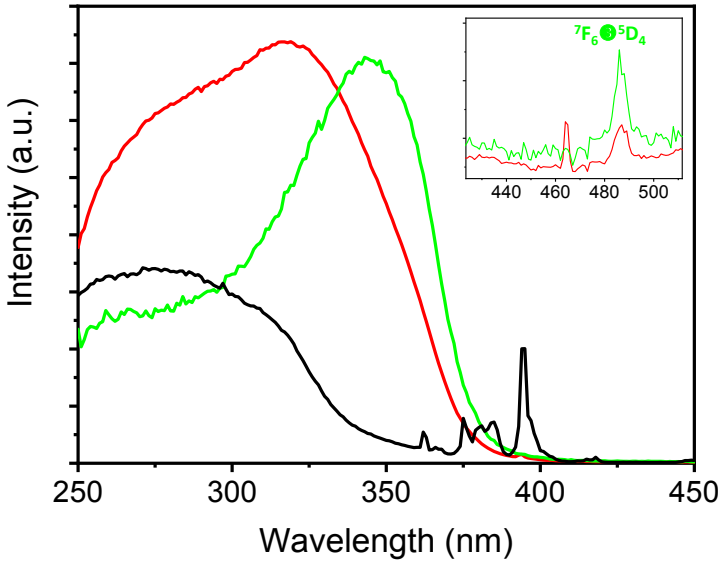

Figure S6: Excitation spectra of **19.5wt%EuW$_{10}$@Tb-TATB** monitored at 541 nm (green line) and at 617 nm (red line), and excitation spectrum of EuW_{10} monitored at 617 nm (black line). (Insert) Evidence of the $^7F_6$✂ $^5D_4$ Tb^{3+} transition in the excitation spectra monitored at 617 nm ($^5D_0$✂ $^7F_2$ Eu^{3+} transition) confirming the presence of the intermolecular Tb^{3+}-to-Eu^{3+} energy transfer.

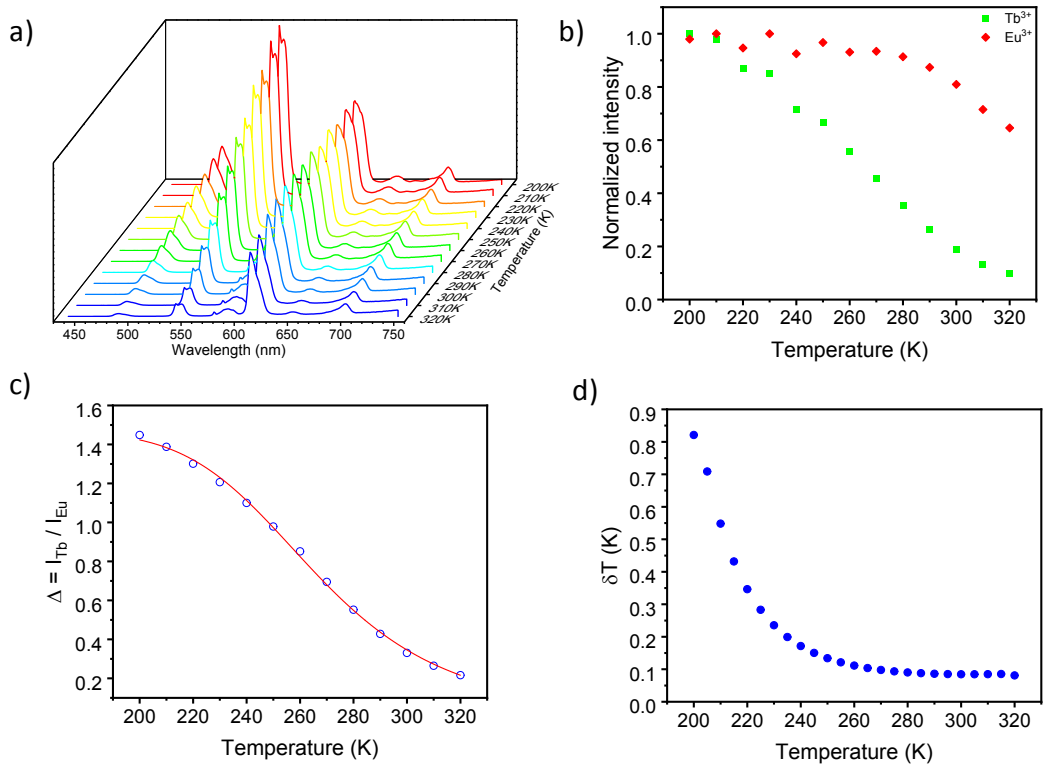

Figure S7: a) Emission spectra of **19.5wt%EuW$_{10}$@Tb-TATB** in the 200-320 K range with the excitation fixed at 330 nm; b) Corresponding temperature dependence of the I_{Tb} (green) and I_{Eu} (red) parameters; c) Corresponding temperature dependence of Δ in the 200-320 K range and Mott-Seitz fit (red line, $R^2 = 0.999$); d) Corresponding temperature uncertainty ($\delta T = 1/S_r \times \delta\Delta/\Delta$). $\delta\Delta/\Delta$ was estimated by the average relative errors in the same temperature range (0.2%).

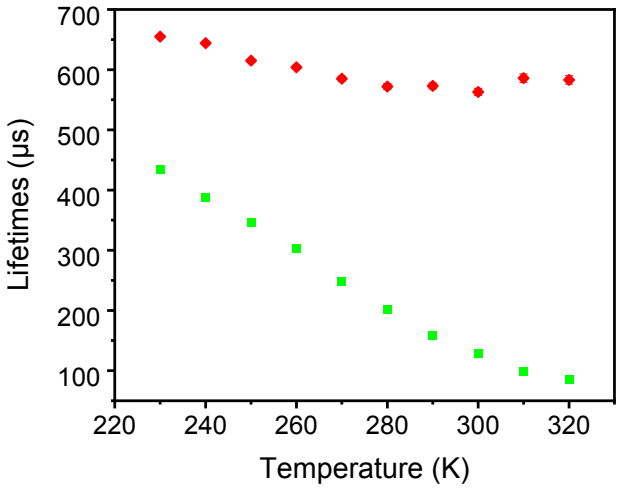

Figure S8: Temperature-dependence of lifetimes of the $^5D_4$ level of Tb^{3+} (green points) and the $^5D_0$ level of Eu^{3+} (red points) for **9.1wt%EuW$_{10}$@Tb-TATB**.

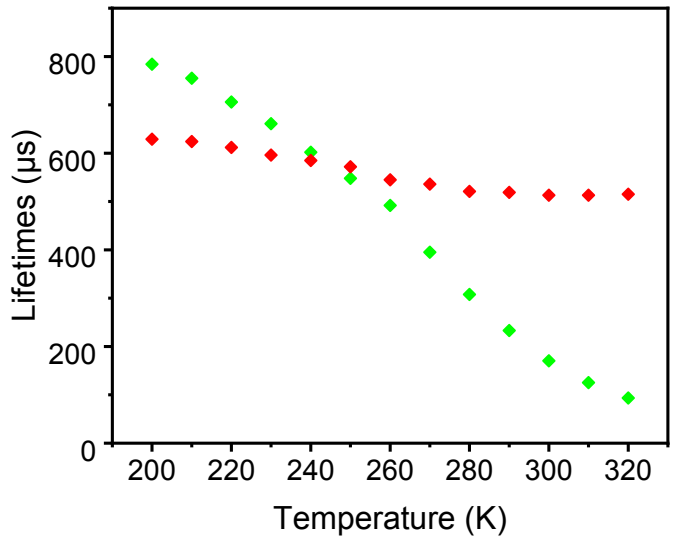

Figure S9: Temperature-dependence of lifetimes of the $^5D_4$ level of Tb^{3+} (green points) and the $^5D_0$ level of Eu^{3+} (red points) for **19.5wt%EuW$_{10}$@Tb-TATB**.

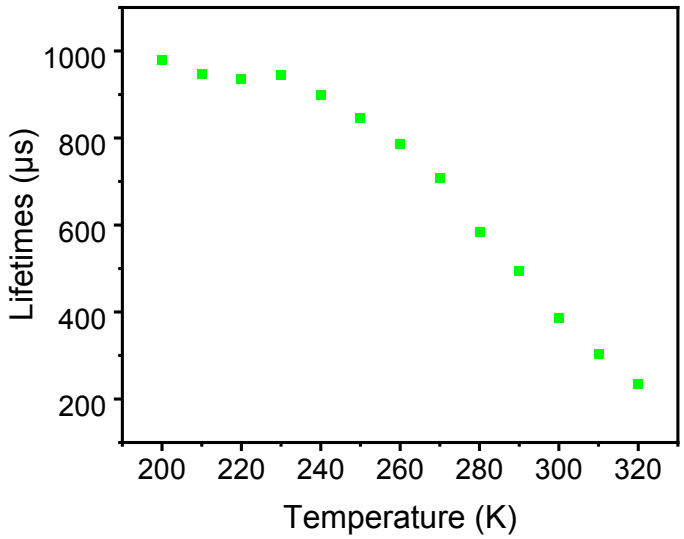

Figure S10: Temperature-dependence of lifetimes of the $^5D_4$ level of Tb^{3+} (green points) for Tb-TATB.

Table S1: Lifetime at room temperature of the $^5D_4$ Tb^{3+} level and the $^5D_0$ Eu^{3+} level, and Tb^{3+}-to-Eu^{3+} energy transfer efficiency in the **Tb-TATB** MOF and both composite materials.

Sample	$^5D_4$ lifetime (545 nm) µs	$^5D_0$ lifetime (615 nm) µs	η_{ET}
Tb-TATB	737 ± 6		
9.1wt%EuW_{10}@Tb-TATB	439 ± 4	620 ± 5	40%
19.5wt%EuW_{10}@Tb-TATB	463 ± 3	809 ±3	37%